CARDIFF UNIVERSITY
PRIFYSGOL CAERDYDD

ORCA – Online Research @ Cardiff

This is an Open Access document downloaded from ORCA, Cardiff University's institutional repository:https://orca.cardiff.ac.uk/id/eprint/99273/

This is the author's version of a work that was submitted to / accepted for publication.

Citation for final published version:

Cuenca, Jerome A. , Slocombe, Daniel Rhys and Porch, Adrian 2017. Temperature correction for cylindrical cavity perturbation measurements. IEEE Transactions on Microwave Theory and Techniques 65 (6) , pp. 2153-2161. 10.1109/TMTT.2017.2652462

Publishers page: http://dx.doi.org/10.1109/TMTT.2017.2652462

Please note:
Changes made as a result of publishing processes such as copy-editing, formatting and page numbers may not be reflected in this version. For the definitive version of this publication, please refer to the published source. You are advised to consult the publisher's version if you wish to cite this paper.

This version is being made available in accordance with publisher policies. See http://orca.cf.ac.uk/policies.html for usage policies. Copyright and moral rights for publications made available in ORCA are retained by the copyright holders.

Temperature Correction for Cylindrical Cavity Perturbation Measurements

Jerome A. Cuenca, Daniel R. Slocombe, and Adrian Porch

***Abstract*— The need for accurate material property measurements using microwave cavities requires a form of compensation to correct for changes in temperature and other external influences. This paper details a method for temperature correcting microwave cavity perturbation measurements by monitoring two modes; one which is perturbed by the sample and one which is not (referred to as a nodal mode). The nodal modes used (TM_{310} and TE_{311} for an axial sample in a cylindrical cavity) are subject only to sample-independent influences. To demonstrate this technique, the bulk permittivity of a PTFE rod has been measured under varying temperature conditions. The results show that without correction, the measured temperature-dependent dielectric constant has large variations associated with the stepped and linear temperature ramping procedures. The corrected response mitigates systematic errors in the real part. However, the correction of the imaginary part requires careful consideration of the mode coupling strength. This paper demonstrates the importance of temperature correction in dynamic cavity perturbation experiments.**

***Index Terms*— Cavity perturbation, microwave material measurements, temperature correction, temperature dependence.**

I. Introduction

THE CAVITY perturbation method is very common for characterizing materials at microwave frequencies because of its precision, simplicity, and noncontact nature. This method involves perturbing a resonant electromagnetic field within a cavity by inserting a sample into the required field region and examining the change in the frequency response of the cavity. Samples, such as those containing ferrous oxides [1], [2] carbon nanotubes [3], oil [4] nanodiamond [5]–[8], bacteria [9], [10], PTFE and common plastics [11], [12], and explosives [13], have all been characterized using this method to infer various properties through changes in microwave complex permittivity and permeability. Due to its noncontact nature, it has also become an effective material probe for measuring chemical reactions in hydrogen storage materials *in situ* [14] and since high-power microwaves can be used for heating, the dependence of the dielectric properties with heating has also been investigated *in situ* using a 100-W cavity system [15], [16].

Manuscript received October 9, 2016; revised December 16, 2016; accepted December 18, 2016. Date of publication March 20, 2017; date of current version June 2, 2017. This work was supported in part by Merck KGaA, Darmstadt, Germany, and in part by the U.K. Engineering and Physical Sciences Research Council under Grant EP/K502819/1. Information on the presented data can be found in the Cardiff University data catalogue at http://doi.org/10.17035/d.2017.0030964432.

The authors are with the School of Engineering, Cardiff University, Cardiff CF24 3AA, U.K. (e-mail: cuencaj@cf.ac.uk; slocombed1@cf.ac.uk; porcha@cf.ac.uk).

Color versions of one or more of the figures in this paper are available online at http://ieeexplore.ieee.org.

Digital Object Identifier 10.1109/TMTT.2017.2652462

With the increasing number of applications for cavity perturbation as a noncontact material probe in chemistry, one must read carefully when dealing with exothermic and endothermic reactions to keep the system stable [17]. Since both the unperturbed resonant frequency and bandwidth are functions of the cavity geometry, the cavity response will change due to the natural thermal expansion and temperature-dependent conductivity of the metal cavity. The change in temperature of a sample can consequently cause the cavity to change resonance frequency through radiative heat transfer. Therefore, the observed shifts in frequency are merely systematic errors as opposed to any change in the dielectric or magnetic property. Thus, when temperature becomes a dependent variable, intrinsic material properties need to be decoupled from system temperature fluctuations. This can be achieved in the cavity perturbation system by *in situ* monitoring of modes where the sample provides minimal perturbation.

Previous studies have already shown that this technique is effective for rectangular type geometries [18], [19]. For dielectric resonator setups, the temperature dependence of the external cavity has already been investigated when extracting temperature coefficients of extremely low loss dielectrics [11], [20], [21]. This paper, however, addresses the conventional cavity perturbation setup, where the sample does not resonate and merely produces a small perturbation in a mode as a result of the boundary conditions of just the cavity.

The novel contribution in this paper is threefold. First, for the cavity correction modes presented, the sample has a minimal perturbation in both the E- and H-fields. The previous studies use modes where the sample still perturbs the H-field in the assumption that the complex permeability is equivalent to air, restricting the measurement to pure dielectrics. Furthermore, the system in this paper has the potential to measure both the temperature-dependent dielectric and magnetic properties.

Second, the system is a hollow cylindrical cavity and exploits the fact that the cavity modes are described by Bessel functions. A cylindrical cavity becomes advantageous in measuring temperature-dependent properties of axial samples because with increasing mode number (and thus Bessel function order), the field maxima are pushed toward the perimeter of the cavity. The higher the mode, the less sensitive it is to the axial sample. Also, for dielectric resonators, the use of correction modes is not possible, since the sample is the resonator or perturbs a large portion of the cavity.

Finally, as a development on previous methods which subtract gradients based on linear coefficients, the proposed method does not rely on previously measured data of

This work is licensed under a Creative Commons Attribution 3.0 License. For more information, see http://creativecommons.org/licenses/by/3.0/

expansion coefficients of known materials. Instead, it uses an intermodal relationship between cavity modes and so corrects for each individual experiment.

In this paper, we have used a selection of cylindrical cavity resonators to demonstrate multimode correction. Section II presents a derivation of the temperature-dependent cavity parameters and the correction modes. Section III presents data and discussions on temperature experiments on three cylindrical cavities; two aluminum cavities which are used in our laboratory for dielectric measurements using the TM_{010} mode and magnetic measurements using the TE_{011} mode, respectively, and a copper cavity similar to the TM_{010} aluminum cavity but with smaller dimensions. The chosen nodal modes are the TM_{m10} and TE_{m11} modes (where $m > 1$).

II. Analysis

In practice, cylindrical cavity measurements are generally achieved by placing a sample in the field in a nondepolarizing or demagnetizing configuration. Hence, this is the reason why modes, such as the TM_{010} and TE_{011} modes, are used for thin rod shaped samples measurements placed axially [22]–[24]. Given that the cavity perturbation method already offers such high sensitivity and minimal sample requirements, the aim of this paper is to demonstrate the measurement of temperature-dependent properties *in situ*, in a temperature varying environment. Several challenges exist with this approach, as it is clear that even though the cavity is mechanically sturdy, it is prone to the effects of thermal stress and temperature-dependent electrical conductivity, as well as changes in antenna geometry and coupling symmetry. These systematic errors will offset the resonant frequency and the bandwidth.

A. Temperature-Dependent Frequency

In a temperature controlled permittivity measurement, we assume the cavity to have a fixed volume, though in the event where the sample is changing temperature and potentially radiating heat, the resultant convection will inevitably create a temperature increase at the cavity walls. This process depends upon the temperature of the sample, the thermal properties of the cavity medium, and the thermal properties of the conducting walls of the cavity. We can further examine the effect of temperature on the cavity by looking at the wave dispersion relation of an air-spaced cylindrical cavity resonator. For TM modes generally, we have

$$f_0 = \frac{c}{2\pi}\sqrt{\left(\frac{k_{mn}}{a(T)}\right)^2 + \left(\frac{p\pi}{l(T)}\right)^2} \tag{1}$$

where c is the speed of light, n, m, and p are the mode integers, k_{nm} is the nth root of the mth order Bessel function of the first kind, and $a(T)$ and $l(T)$ are the temperature-dependent radius and height of the cavity, respectively. The temperature-dependent dimensions of the cavity can be described by a linear thermal expansion approximation

$$a(T) \approx a_0(1 + \alpha_c \Delta T) \tag{2}$$

$$l(T) \approx l_0(1 + \alpha_c \Delta T) \tag{3}$$

where a_0 and l_0 are the initial dimension lengths, ΔT is the change in temperature, and α_c is the linear thermal expansion coefficient of the cavity metal. Using the first-order partial derivatives, the change in resonant frequency due to an increased temperature can be given by

$$\frac{\partial f_0}{\partial T} \approx \frac{\partial f}{\partial a}\frac{\partial a}{\partial T} + \frac{\partial f}{\partial l}\frac{\partial l}{\partial T} \approx \alpha_c\left(\frac{\partial f}{\partial a}a_0 + \frac{\partial f}{\partial l}l_0\right). \tag{4}$$

Evaluating each partial derivative and taking discrete measurements of frequency and temperature, we find that the fractional shift in frequency is

$$\frac{\Delta f_0}{f_0} \approx -\alpha_c\left(\frac{c}{2\pi f_0}\right)^2\left(\frac{k_{nm}^2}{a_0^2} + \frac{p^2\pi^2}{l_0^2}\right)\Delta T \approx -\alpha_c \Delta T. \tag{5}$$

This shows that any fractional increase in frequency with temperature is simply proportional to the linear thermal expansion coefficient of the cavity material. Therefore, if the cavity changes temperature, the change in frequency as a function of temperature will have a gradient equal to $-\alpha_c f_0$. Correction of TM_{010} measurements simply involves removing this gradient [25]. However, since the geometry of the cavity is not ideal due to holes for the sample and coupling, α_c may be different for each mode and consequently simple subtraction will not suffice. A more reasonable assumption is that the relationship between each of the modes (or the difference between the gradients of each mode) is the same. The novel aspect of this paper is this principle.

B. Temperature-Dependent Bandwidth

A similar derivation for bandwidth can be achieved using the well-known quality factor equation, where the power that is lost is caused by the electrical resistance in the cavity metal

$$Q_0 = \frac{\text{Energy stored}}{\text{Power losses}} = \frac{\mu_0 \int_{V_c} H_{\mathrm{cav}}^2 dV}{R_s \int_{S_c} H_{\mathrm{cav}}^2 dS} \tag{6}$$

where Q_0 is the unloaded quality factor, R_s is the surface resistance of the cavity metal, S_c and V_c are the surface area and volume of the cavity, respectively, and H_{cav} is the spatially dependent magnetic field. Evaluating the numerator of (6) gives

$$\mu_0 \int_{V_c} H_{\mathrm{cav}}^2 dV = \begin{cases} \mu_0 U_{mnp} V_c(T), & p = 0 \\ \dfrac{1}{2}\mu_0 U_{mnp} V_c(T), & p \geq 1 \end{cases} \tag{7}$$

where U_{mnp} is the volume fraction of the cavity that is occupied by the squared magnetic field. Evaluating the denominator of (6) gives

$$R_s \int_{S_c} H_{\mathrm{cav}}^2 dS = \begin{cases} V_c(T) R_s(T)\left[\dfrac{1}{a(T)} + \dfrac{1}{l(T)}\right], & p = 0 \\ \dfrac{V_c(T) R_s(T)}{2}\left[\dfrac{1}{a(T)} + \dfrac{2}{l(T)}\right], & p \geq 1. \end{cases} \tag{8}$$

Surface resistance is defined as $R_s(T) = (\pi \mu_0 \rho(T) f(T))^{1/2}$, where $\rho\ (T)$ is the temperature-dependent resistivity of the

cavity walls. Substituting (7) and (8) into (6) yields an equation for the theoretical unloaded bandwidth

$$\mathrm{BW}_0(T) = \begin{cases} \sqrt{\dfrac{\rho\ (T) f_0(T)}{\mu_0 \pi}} \left(\dfrac{1}{a(T)} + \dfrac{1}{l(T)} \right), & p = 0 \\ \sqrt{\dfrac{\rho\ (T) f_0(T)}{\mu_0 \pi}} \left(\dfrac{1}{a(T)} + \dfrac{2}{l(T)} \right), & p = 1. \end{cases} \tag{9}$$

This equation defines the minimum theoretical bandwidth for a cylindrical cavity resonator constructed out of a material with an electrical resistivity $\rho\ (T)$; an aluminum cavity designed for a TM_{010} mode at 2.495 GHz ($a = 46$ mm and $l = 40$ mm), for example, would give a theoretical minimum bandwidth of approximately 190 kHz ($Q_0 \approx 1.3 \times 10^4$). In practice, however, the aluminum surface quality is not perfect and roughness coupled with a reduction in the electrical quality due to dislocations will greatly increase this value. Using the same approach as the temperature-dependent frequency derivation

$$\frac{\partial \mathrm{BW}}{\partial T} \approx \frac{\partial \mathrm{BW}}{\partial f}\frac{\partial f}{\partial T} + \frac{\partial \mathrm{BW}}{\partial a}\frac{\partial a}{\partial T} + \frac{\partial \mathrm{BW}}{\partial l}\frac{\partial l}{\partial T} + \frac{\partial \mathrm{BW}}{\partial \rho}\frac{\partial \rho}{\partial T}. \tag{10}$$

Assuming that $\rho\ (T)$ is a linear function of temperature such that $(\partial\rho/\partial T) \cong \beta_c$, the partial derivatives give the following equation-dependent upon geometrical expansion and resistivity:

$$\frac{\Delta \mathrm{BW}}{\mathrm{BW}_0} \approx \frac{1}{2}(\beta_c - 3\alpha_c)\Delta T \approx \frac{1}{2}\beta_c \Delta T. \tag{11}$$

Thus, theoretical unloaded bandwidth linearly increases with increasing resistivity and decreases with geometrical expansion of the volume. Typically for metals, the coefficient of resistivity is three orders of magnitude greater than thermal expansion, hence the contribution from α is much smaller (for aluminum, $\beta_c \approx 4 \times 10^{-3}$/°C while $\alpha_c \approx 22 \times 10^{-6}$/°C). This equation, however, does not consider effects due to coupling strength into the resonator and its symmetry. The cavity coupling strengths are also complex functions of temperature, since the geometry of the coupling structures will expand and change resistance. Because of this, the difference in the bandwidth gradients for each mode may differ greatly. However, if the difference between each mode is constant and known then correction can still be achieved. It must also be stipulated that the variation in bandwidth may be as high 1 kHz, as is in our system described later, which gives a variation of 5×10^{-3}/°C, a value as large as β_c. This means that only large changes in resistivity can be measured while the effects of the temperature-dependent coupling may dominate. More on the reliability of bandwidth correction is explained in Section III-D.

C. Nodal Mode Correction

From (5), all resonant frequencies of the cavity will drift up and down with temperature by the same fractional amount. The frequency and bandwidth measurement of the TM_{010} mode whilst the temperature is varying is in error by a gradient which is dependent on thermal expansion and resistivity and so a simple subtraction of this gradient is required. A more robust method is to use a mode where the sample has minimal perturbation, referred to in this paper as a nodal mode. Therefore, the corrected frequency shift (attributed to just the properties of the sample) is simply the fractional frequency shift of the sample measurement mode $\Delta f/f_{\mathrm{sample}}$ minus the fractional frequency shift of the nodal mode ($\Delta f/f_{\mathrm{node}}$). The fractional frequency shift of the measurement and nodal modes with temperature can be modeled as follows:

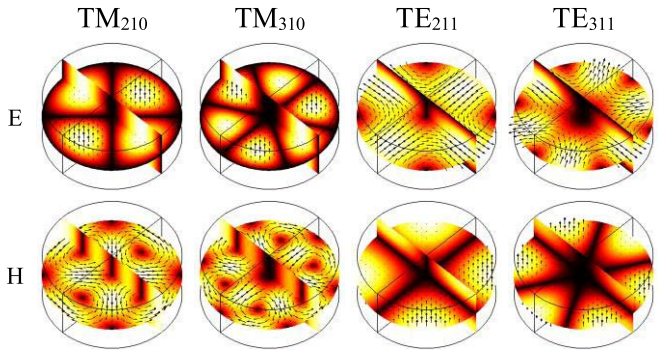

Fig. 1. Field distributions (from left to right) of TM_{210}, TM_{310}, TE_{211}, and TE_{311} using COMSOL multiphysics (cavity dimensions of $a = 46$ mm and $l = 40$ mm). The top and bottom rows depict E- and H-field distributions, respectively. Notice that as m increases, the axial node (dark region) gets broader, whilst the field maxima (light regions) tend toward the perimeter owing to the distributions being described by Bessel functions.

$$\frac{\Delta f_{010}(T)}{f_{010}(0)} \approx \frac{\Delta f_{\mathrm{k}}\ (T)}{f_{\mathrm{k}}\ (0)} - (\alpha_c + \kappa_{010})\Delta T + \kappa_{\mathrm{err}}(T) \tag{12}$$

$$\frac{\Delta f_{m10}(T)}{f_{m10}(0)} \approx -(\alpha_c + \kappa_{m10})\Delta T + \kappa_{\mathrm{err}}(T) \tag{13}$$

where the fractional frequency shift denoted by k is the shift caused by the perturbation, κ_{010} and κ_{m10} are given as the differences in gradient from the intrinsic thermal expansion coefficient of the metal and the observed mode, and κ_{err} is a systematic thermal expansion error in the experiment. Subtracting (13) from (12)

$$\frac{\Delta f_{010}(T)}{f_{010}(0)} - \frac{\Delta f_{m10}(T)}{f_{m10}(0)} \approx \frac{\Delta f_{\mathrm{k}}(T)}{f_{\mathrm{k}}(0)} - (\kappa_{010} - \kappa_{m10})\Delta T \tag{14}$$

the thermal expansion error in the experiment is eliminated although, the gradient terms remain. These are simply removed using subtraction with the unperturbed state

$$\frac{\Delta f_s(T)}{f_s(0)} \approx \left[\frac{\Delta f_{010,s}(T)}{f_{010,s}(0)} - \frac{\Delta f_{m10,s}(T)}{f_{m10,s}(0)}\right] - \left[\frac{\Delta f_{010,u}(T)}{f_{010,u}(0)} - \frac{\Delta f_{m10,u}(T)}{f_{m10,u}(0)}\right] \tag{15}$$

where u and s denote the temperature-dependent fractional frequency shift of the unperturbed and perturbed cavity, respectively. Through cavity perturbation, the change in permittivity with respect to a reference temperature is, therefore,

$$\varepsilon_1(T) \approx -2\left[\frac{f_s(T) - f_0(T)}{f_s(0)}\right]\frac{V_c}{V_s}G_{mnp} + 1 \tag{16}$$

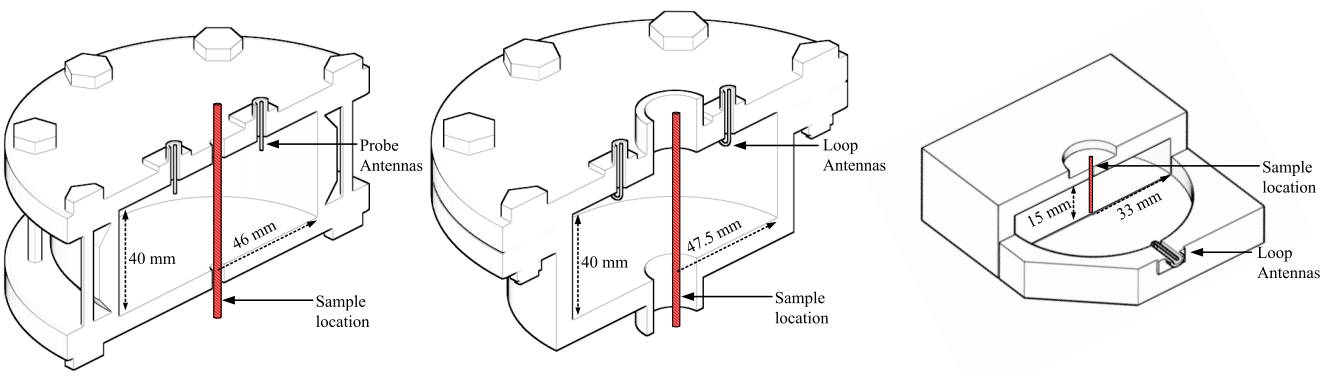

Fig. 2. Cut views of the cylindrical cavities used in this paper. Aluminum TM-probe antenna cavity (left) couples into the E-field of TM modes to provide dielectric measurements. Aluminum TE-loop antenna cavity (middle) couples into the H-field of TE modes to provide magnetic measurements. A copper side-loop coupled cavity couples into TM modes to provide dielectric measurements whilst also coupling to some TE nodal modes.

where synonymously, the imaginary part can be obtained from the corrected bandwidth or quality factor

$$\varepsilon_2(T) \approx \left[\frac{1}{Q_s(T)} - \frac{1}{Q_0(T)}\right]\frac{V_c}{V_s}G_{mnp}. \tag{17}$$

This approach has a distinct advantage over a simple gradient subtraction in that it corrects for any geometrical expansion at the measurement time. In the simple case, while it is reasonable to assume that the cavity homogenously changes temperature due to the high thermal conductivity of the metal, it is also assumed that the structural thermal expansion happens instantaneously for a given temperature increase. This is of course not the case and there is a finite time required for the cavity to expand which the nodal correction method does take into account since the correction is performed at the time of measurement. For bandwidth, however, it is not as simple, since each mode will be affected by its own mode-dependent coupling strength. This can be mitigated somewhat by correcting for unloaded bandwidth [26].

There are numerous modes, which have a node on the axis. This can be realized by recalling that all E- and H-field components in cylindrical modes are dependent on mth order Bessel functions of the first kind [27]. Taking r to be the radial distance from the center of the cavity, any mode where $J_m(r = 0)$ and $J'_m(r = 0)$ are equal to zero will yield a possible nodal measurement mode. Examples of these modes are shown in Fig. 1. As m increases, the central node spot gets broader and the mode is, therefore, less sensitive to the sample, although as mode number increases, interference from other modes starts to become considerable.

The existence of these nodal modes depends upon whether the coupling structures excite them. Open circuit coaxial probes (E-field antennas) are used to excite TM modes and short circuited coaxial loops (H-field antennas) are used to excite TE modes. Placing these antennas on the end plates and near the axis of the cavity allows coupling into the TM_{0np} and TE_{0np} modes for the E- and H-field antennas, respectively. In this position, some of the nodal modes are also excited. However, since the field maxima tends toward the perimeter with increasing m, much higher order modes are not excited. If the coupling antennas are located on the side of the cavity (i.e., H-field coupling to the TM_{010} mode or E-field coupling to the TE_{111} mode) then this configuration will excite the higher nodal modes. The cavities used in this paper are shown in Fig. 2; an E-field coupled TM cavity, an H-field coupled TE cavity, and an H-field coupled TM cavity. The first two nodal modes of the TM cavities are the TM_{210} and TM_{310} modes. For the H-field TE cavity, the first two nodal modes are the TE_{211} and TE_{311} modes.

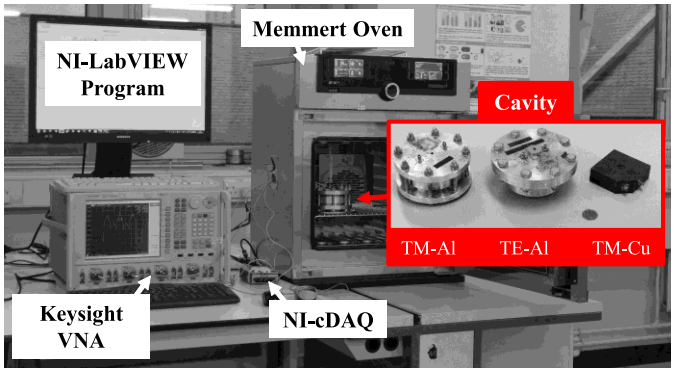

Fig. 3. Photograph of the experimental setup with inset showing the cavities used in this paper (coin is a 50-pence piece). A Keysight Technologies VNA (PNA-L N232A) is used to measure the cavity resonance. A Memmert oven is used change the ambient temperature of the cavity. Temperature sensors are attached to the cavity and interfaced to a PC via a NI-cDAQ-9171. Temperature and S21 data are recorded using a program written using NI–LabVIEW.

III. Experiment and Discussion

The experiments were conducted with the two aluminum cavities and one copper cavity, schematics shown in Fig. 2. The first cavity is designed to excite TM modes using E-field antennas and the second is designed to excite TE modes using H-field coupling. The copper cavity excites both TE and TM modes due to its side H-field antennas and was used to demonstrate the measurements of the thermal properties of a different material to aluminum. A photograph of the experimental setup is shown in Fig. 3. Temperature ramps were achieved by placing the cavity inside of a Memmert UF30 laboratory oven. The temperature profiles (stepped and ramped) were

TABLE I
FRACTIONAL FREQUENCY SHIFTS OF THE NODAL MODES IN THE ALUMINUM CAVITIES

Mode	$\Delta f/f_0$ ($\times 10^{-6}$)	$\Delta BW/BW_0$ ($\times 10^{-3}$)
TM_{210}	52 ± 1	-1 ± 4
TM_{310}	0.4 ± 0.3	3.1 ± 3
TE_{211}	-9.8 ± 0.7	0.2 ± 2
TE_{311}	-0.3 ± 0.5	2 ± 4

Errors are the standard deviations for three separate measurements of the 3 mm diameter copper rod plus the measurement error of frequency or bandwidth. Negative values denote downward shifts while positive values denote upward shifts.

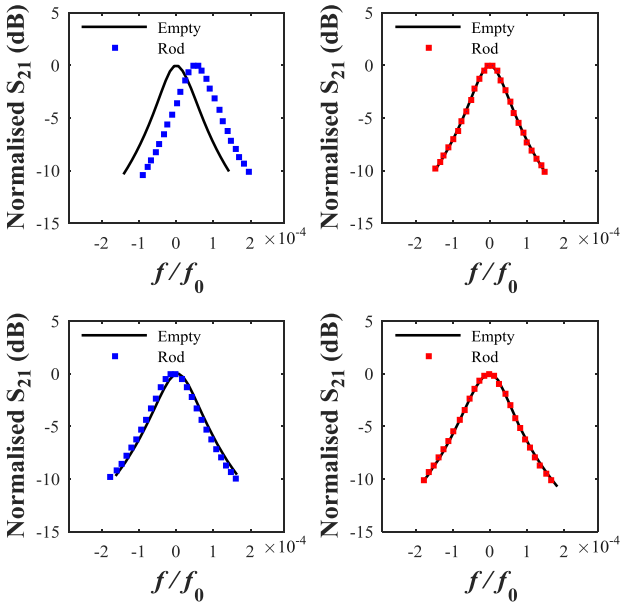

Fig. 4. Normalized S_{21} traces against changes in fractional frequency with and without the copper rod of the TM_{210} (top-left), TM_{310} (top-right), TE_{211} (bottom-left), and TE_{311} modes (bottom-right).

programmed using software provided by the manufacturer. The resonant frequency and bandwidth were recorded using standard transmission measurements (i.e., S21), obtained using a Keysight Technologies VNA (PNA-L N5232A) with RF cables provided by RF COM. The temperature of the cavity was obtained using two Omega PT100 temperature sensors placed on the walls of the cavity and a National Instruments (NI) cDAQ-9171. The VNA and cDAQ were interfaced with the PC and a program written using NI LabVIEW provided automated data recording over long periods.

A. Metal Rod Perturbation

First, to test the effectiveness of the nodal modes, a copper rod with a diameter of 3 mm was placed at the sample location of the aluminum cavities. The differences in resonant frequency after perturbation are given in Table I and the resonant traces are shown in Fig. 4. For the TM cavity, this perturbation essentially destroys the resonance of the TM_{010} mode as the maximum E-field along the axis is forced to zero. This completely supresses the mode, since an E-field cannot exist parallel to a metal interface. For the TE cavity, the H-field in the TE_{011} mode is forced to zero at the center of the cavity, but the distribution is not grossly affected. In this case, the H-field perturbation by the metal rod represents the maximum possible perturbation of a magnetic sample material, since the rod completely screens the H-field. Thus, a metal rod perturbation will give an indication as to whether the observed mode is a nodal mode if the measured frequency and bandwidth shifts are very small. Using curve fitting, the fractional frequency can be measured with a maximum error across the modes of 2×10^{-7} (for example, the TE_{211} mode has a 1-kHz variation around a 4.83-GHz resonance). For bandwidth, the maximum curve fitting error across all of the modes is approximately 4×10^{-3} (1-kHz variation for a typical quality factor of 9×10^3). The results show that TM_{210} is partially perturbed although this is only a maximum fractional shift of 5.2×10^{-5}. This shift is also upward, implying this small perturbation is in the H-field, which is expected for TM modes due to some magnetic field encroaching near to the axis of the cavity, as shown in Fig. 1. The change, however, in TM_{310} is much less affected by the sample at only an upward fractional shift of 4×10^{-7}, which is approaching the curve fitting measurement error. This is expected, since the energy density fraction where the 3-mm metal rod occupies is at greater in the TM_{210} mode as compared with the TM_{310} mode (verified with COMSOL). This makes these two modes ideal for the correction of the TM_{010} mode. The TE_{211} and TE_{311} modes yield shifts of -9.8×10^{-6} and -3×10^{-7}, respectively. This is expected again, since the energy fraction in the TE_{211} mode is greater than for TE_{311} mode. The shift downward is implicit of a slight perturbation into the E-field. The fractional changes in bandwidth are much more sensitive to the sample location, though still of the same order of the measurement error, as shown in Table I. Notice that the bandwidth decreases in the TM modes, which is implicit of a decrease in the power losses in the cavity. This can be explained by the fact that the rod is made of copper and has a higher conductivity than aluminum. Hence, the induced surface current in a better conductor caused by the slight H-field perturbation actually increases the quality factor.

B. Ambient Temperature Drift

Both the aluminum TE cavity and the copper cavity were measured over a period of 4 h on separate occasions in the laboratory to study the effects of the ambient temperature on the nodal and sample measurement modes from 3 to 10 GHz. The results in Fig. 5 show that for a given cavity, all modes drift with the same fractional frequency shift with temperature. The bandwidth drift was below the noise floor of the measurements and yielded a stable response. This is because the sensitivity is much less as the fractional variations are with respect to kilohertz as opposed to gigahertz. The temperature differences are also very small and thus the resistivity will not change by much. This experiment demonstrates the sensitivity of the frequency measurement and that all of the resonant frequencies are inherently linked through geometrical expansion, as described previously in (5).

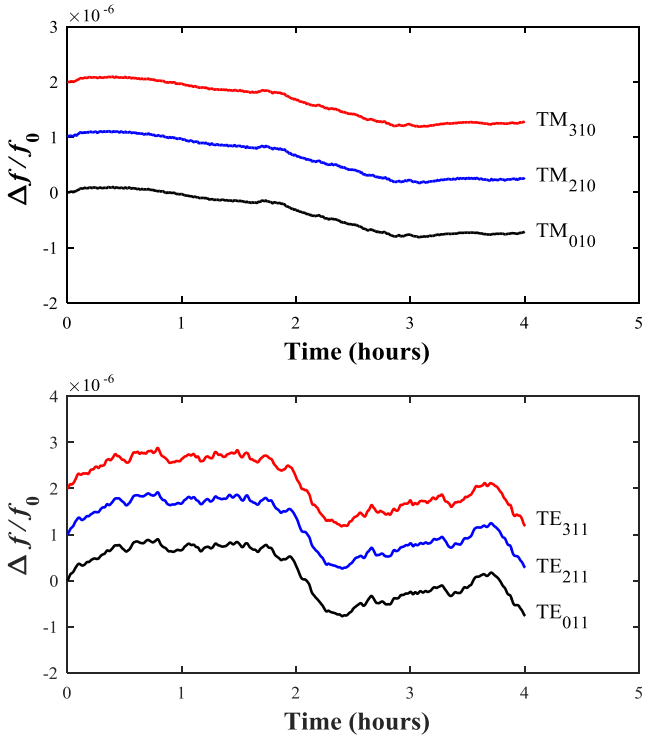

Fig. 5. Fractional frequency shifts in the laboratory for 4 h of the copper cavity (top) and the aluminum TE cavity (bottom). Traces have been separated by 1×10^{-6} for visibility.

C. Temperature Ramps

A temperature ramp profile of 30 °C–80 °C at 1 °C per minute was imposed on the cavity to prove the nodal mode principle. While a small temperature range has been used owing to laboratory limitations, this cavity thermal expansion correction method will also work over a much wider temperature range, at both lower and higher temperatures. This experiment demonstrates the linear relationship between frequency and temperature.

Fig. 6 shows the ramping results while Table II shows the linear fits. The gradients show the approximate values for the linear thermal expansion coefficients of their respective metals as expected from (5). The TM_{010} mode of the aluminum TM cavity has a slightly smaller than expected value of 19.3×10^{-6}/°C, though this is not an issue, since it is the relationship between this mode and the nodal modes that is important. The TM_{210} and TM_{310} modes yield gradients much closer to expected values. There is also a discrepancy in the copper TM cavity measurements, where the gradient of the TM_{210} mode is much smaller than the others. This is most likely due to this mode having a slightly asymmetrical resonance because of three coupling port holes on the cavity.

Resistivity measurements were variable, owing to the issues of sensitivity in measuring the fractional bandwidth shifts combined with the temperature dependence of the coupling antennas. Both the Al TE cavity and the C_u TM cavity have loop coupling structures, which will expand as temperature increases, thereby causing a temperature-dependant coupling strength. The only repeatable measurements are those for the TM cavity, as shown in Table II. These values are similar to those reported of 3.6×10^{-3}/°C with discrepancies again associated with the temperature dependence of the coupling antennas.

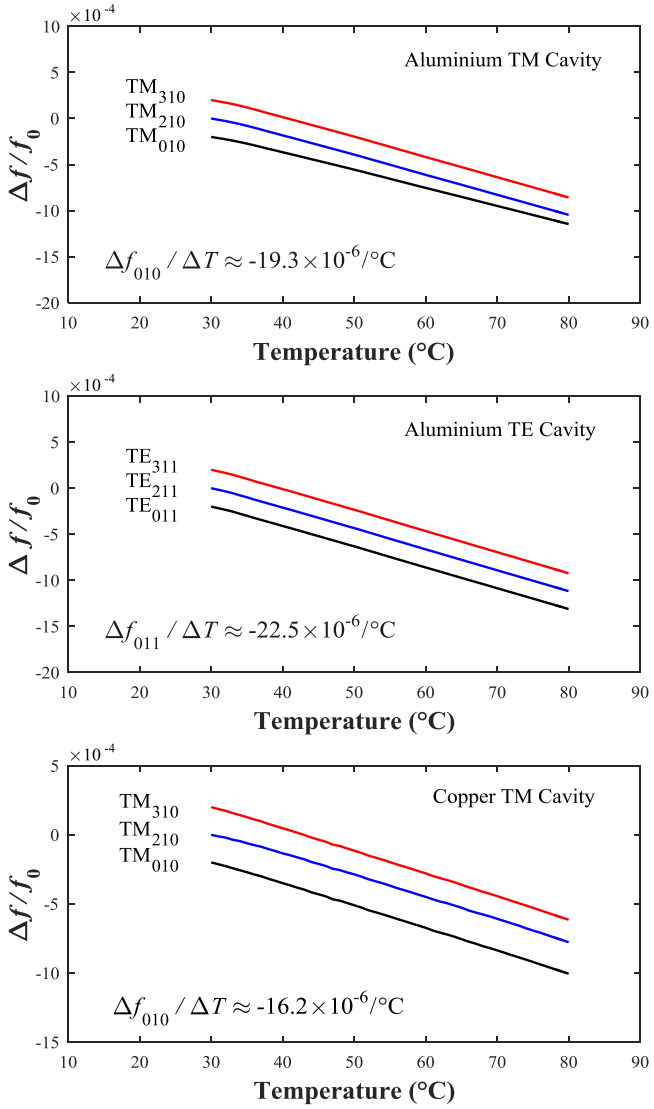

Fig. 6. Temperature-dependent change in fractional frequency shifts of (top) aluminum TM cavity (middle) aluminum TE cavity, and (bottom) copper TM cavity. Plots have been separated for visibility.

TABLE II
OBSERVED THERMAL EXPANSION COEFFICIENTS

Mode	Cavity Material	Frequency (GHz)	α_c (×10^{-6}/°C) $R^2 > 0.99$	β_c (×10^{-3}/°C) $R^2 > 0.99$
TM_{010}	Al	2.49	19.3	3.1
TM_{210}	Al	5.33	21.3	2.2
TM_{310}	Al	6.61	21.6	2.4
TM_{010}	Cu	3.49	16.2	-
TM_{210}	Cu	7.45	15.8	-
TM_{310}	Cu	9.26	16.4	-
TE_{011}	Al	5.36	22.5	-
TE_{211}	Al	4.83	22.6	-
TE_{311}	Al	5.64	22.7	-

Calculated thermal expansion coefficients from the temperature dependent resonant frequency of each cavity mode.

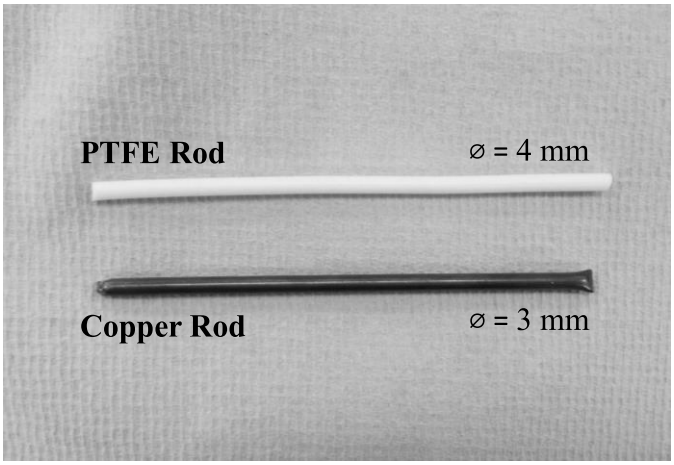

Fig. 7. Photograph of the rod samples used in this paper. The copper rod is used in the metal rod perturbation experiments while the PTFE rod is used in the sample temperature ramping experiments.

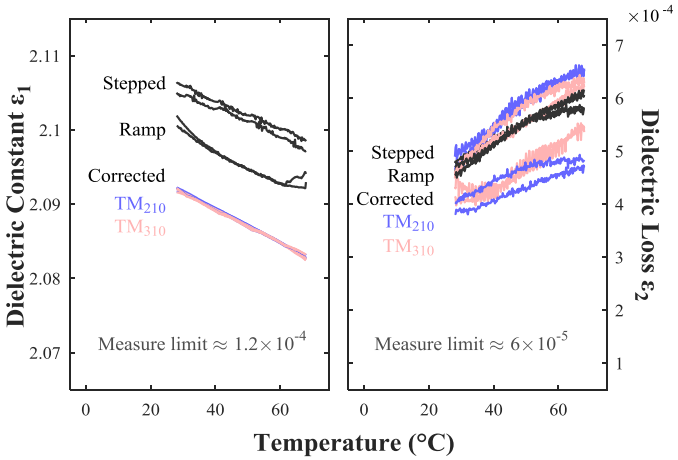

Fig. 8. Calculated temperature-dependent effective complex permittivity of PTFE rod using both stepped and linear ramping profiles. The uncorrected temperature ramps are shown in black, which show varying temperature-dependent behavior owing to the profile used. TM_{210} and TM_{310} corrected ramps are shown in lighter shades. Regardless of ramp profile, the correction gives similar results for the real part, but variation in the imaginary.

This experiment demonstrates a pertinent result in that these modes are all linearly dependent on each other through their own thermal expansion coefficient and, therefore, if the volume of the cavity suddenly changes due to temperature, then other modes can be measured to infer this volume change.

D. Sample and Tube Temperature Ramps

The temperature-dependent complex permittivity of a PTFE rod was measured. This is simply to demonstrate the capability to exclusively extract the temperature-dependent dielectric properties of a sample whilst negating any systematic fluctuations. First, to ensure that any measured temperature-dependent response was due to the sample, ramping experiments were carried out on an empty cavity followed by the sample perturbed cavity. Experiments were conducted using the TM aluminum cavity and the PTFE rod (shown in Fig. 7). The complex permittivity was calculated using the usual cavity perturbation approach given in (16) using linear interpolation at each temperature. In order to induce a systematic error related to thermal expansion, both a linear ramp as well as a stepped profile was conducted. As stated in Section II-C, in an ideal case, the change in temperature of the cavity should result in an instantaneous change in frequency and bandwidth which is not the case because while the thermal conductivity is high, the mechanical deformation has an associated delay or "thermal lag." Two linear ramps and two stepped ramps (at 10 °C steps with a dwell time of 1 h) were conducted starting from 30 °C and 70 °C, where the reference frequencies and bandwidths for the correction method are static values taken at the beginning of the experiment.

The measurements of the PTFE ramps are shown in Fig. 8. Without any correction, the observed dielectric constant decreases with temperature, which is congruent to results already reported [11]. Interestingly, the stepped temperature ramps show different values to those given in the linear ramp. The stepped response yields a linearly decreasing trend, however, there is a noticeable ripple within the data, associated with the stepped ramp profile; noticeable features can be seen at each 10 °C plateau in the dielectric constant. The linear ramp response shows different absolute values. The reason for this is that the recorded temperature at the aluminum surface does not necessarily mean that the equivalent mechanical thermal expansion of the cavity has occurred yet. Hence, when the perturbation equations are used, the cavity volume of the unperturbed state is not the same as the volume when perturbed.

The corrected results, however, are almost equal with a very little difference between the correction modes used (TM_{210} and TM_{310}) and a very little difference between ramping profiles. Again, the absolute values and decreasing trend are similar to the reported values of approximately 2.02 to 2.09 although at a slightly higher frequency of 10 GHz [11]. With the correction procedure, it is shown that finer temperature steps can be used and minute fluctuations in resonant frequency can be corrected. This is because the reference frequencies are static values, taken at a known temperature, and therefore, a reference volume. For the dynamic measurements of dielectric constant, it is clear that the profile must be accounted for to avoid erroneous data.

The loss measurements for PTFE, however, are not as well corrected as the dielectric constant. First, it must be stated that this material has a very low loss tangent and the variations in loss with temperature may seem to increase, but the observed changes approach the measurement limit of this system, as shown in Fig. 8. Second, while the corrected data are erroneous, it actually allows one to understand the limitations behind this correction method. The correction seemingly increases the error on the measurement, where the original traces show repeatable data and the corrected measurements show the opposite. The reason for this is vastly due to the temperature dependence of the coupling structures. As mentioned previously, the coupling antennas are also functions of temperature, and their effects are more profound as their coupling strength increases. In this experiment, antennas have been designed to excite all three of these modes, however,

the coupling strengths (inferred by the magnitude of the resonant peaks in an S_{21} measurement) are much stronger for the correction modes. The magnitude at resonance for TM_{010} is approximately -30 dB while TM_{210} and TM_{310} have magnitudes at approximately -12 and -10 dB, respectively. This means that the influences from the coupling structure on the bandwidth measurements are approximately 0.1%, 6%, and 10%, all of which are greater than the measurement errors given in Table I. This is most likely responsible for the response given in Fig. 8 in the imaginary part. Hence, to use the correction method, the coupling strength into each mode must be minimized, although this is a challenging task, since reducing the strength of the nodal modes will inherently reduce the detectable peak of the measurement mode (TM_{010}) toward the noise floor of the VNA. Ultimately, this creates further difficulties in the temperature-dependent measurement of low loss materials.

IV. Conclusion

In conclusion, microwave cavity perturbation measurements can be corrected by monitoring specific resonant cavity modes. The TM_{210} and TM_{310} modes have been investigated to correct TM_{010} measurements due to their insensitivity to the axial sample. The measurements show that the cavity modes are insensitive to the sample location on the axis. The cavity modes are linked geometrically through linear thermal expansion, though these gradients can vary across the modes and offsets may be apparent. The presented results demonstrate that the nodal correction method can effectively account for any external temperature related influences that affect the cavity volume during perturbation measurements. The analysis presented in Section II-C states that the temperature related offsets ($\kappa_{010} - \kappa_{m10}$) may be accounted for through subtraction. Hence, the biggest limitation in this method is that the unperturbed and perturbed states must be conducted with the same cavity as to eliminate the ($\kappa_{010} + \kappa_{m10}$) term. For example, one cannot use two cavities to measure the unperturbed and perturbed states at the same time as to save time on the experiment. Even if the cavities are designed to the same dimensions, any manufacturing errors would result in differing κ values: ($\kappa_{010,u} - \kappa_{m10,u}$) for unperturbed and ($\kappa_{010,p} - \kappa_{m10,p}$) for perturbed. Thus, these terms do not cancel each other out.

While effective for dielectric constant, this correction method must be used with caution on strongly coupled resonators, since the temperature dependence of the coupling structures can dominate the corrected response, leading to erroneous results. With this in mind, it must be advised that any temperature ramping experiments must be approached with caution, and the effects of the probing system need to be accounted for before any concrete data can be presented.

References

[1] J. A. Cuenca *et al.*, "Study of the magnetite to maghemite transition using microwave permittivity and permeability measurements," *J. Phys. Condens. Matter*, vol. 28, no. 10, p. 106002, Feb. 2016.

[2] U. Raveendranath and K. T. Mathew, "New cavity perturbation technique for measuring complex permeability of ferrite materials," *Microw. Opt. Technol. Lett.*, vol. 18, no. 4, pp. 241–243, Jul. 1998.

[3] A. Porch, D. I. Odili, and P. A. Childs, "Microwave characterisation of carbon nanotube powders," *Nanosc. Res. Lett.*, vol. 7, no. 1, p. 429, Aug. 2012.

[4] A. Porch *et al.*, "Microwave treatment in oil refining," *Appl. Petrochem. Res.*, vol. 2, no. 1, pp. 37–44, Sep. 2012.

[5] J. A. Cuenca, E. Thomas, S. Mandal, O. Williams, and A. Porch, "Broadband microwave measurements of nanodiamond," in *Proc. Asia–Pacific Microw. Conf. (APMC)*, Nov. 2014, pp. 441–443.

[6] J. A. Cuenca, E. Thomas, S. Mandal, O. Williams, and A. Porch, "Investigating the broadband microwave absorption of nanodiamond impurities," *IEEE Trans. Microw. Theory Techn.*, vol. 63, no. 12, pp. 4110–4118, Dec. 2015.

[7] J. A. Cuenca, E. Thomas, S. Mandal, O. Williams, and A. Porch, "Microwave determination of sp^2 carbon fraction in nanodiamond powders," *Carbon J.*, vol. 81, no. 1, pp. 174–178, Jan. 2015.

[8] D. Slocombe, A. Porch, E. Bustarret, and O. A. Williams, "Microwave properties of nanodiamond particles," *Appl. Phys. Lett.*, vol. 102, no. 24, p. 244102, Jun. 2013.

[9] C. F. Williams, G. M. Geroni, A. Pirog, D. Lloyd, J. Lees, and A. Porch, "The separated electric and magnetic field responses of luminescent bacteria exposed to pulsed microwave irradiation," *Appl. Phys. Lett.*, vol. 109, no. 9, p. 93701, Aug. 2016.

[10] C. F. Williams *et al.*, "What the deep sea can tell us about microwaves," in *IEEE MTT-S Int. Microw. Symp. Dig.*, May 2016, pp. 1–4.

[11] B. Riddle, J. Baker-Jarvis, and J. Krupka, "Complex permittivity measurements of common plastics over variable temperatures," *IEEE Trans. Microw. Theory Techn.*, vol. 51, no. 3, pp. 727–733, Mar. 2003.

[12] G. Zhang, S. Nakaoka, and Y. Kobayashi, "Millimeter wave measurements of temperature dependence of complex permittivity of dielectric plates by the cavity resonance method," in *Proc. Asia–Pacific Microw. Conf. (APMC)*, vol. 3. Dec. 1997, pp. 913–916.

[13] A. L. H. Duque, W. L. Perry, and C. M. Anderson-Cook, "Complex microwave permittivity of secondary high explosives," *Propellants, Explos. Pyrotech.*, vol. 39, no. 2, pp. 275–283, Apr. 2014.

[14] J. Hartley, A. Porch, and M. Jones, "A non-invasive microwave method for assessing solid-state ammonia storage," *Sens. Actuators B, Chem.*, vol. 210, pp. 726–730, Apr. 2015.

[15] Y. Guan and Y. Nikawa, "Measurement of temperature-dependent complex permittivity for materials using cylindrical resonator under microwave irradiation," *Electron. Commun. Jpn. (Electron.)*, vol. 90, no. 11, pp. 1–8, Nov. 2007.

[16] T. Kobayashi and Y. Nikawa, "Dynamic measurement of temperature dependent permittivity of liquid material using microwaves," in *Proc. Asia–Pacific Microw. Conf. (APMC)*, Dec. 2010, pp. 1368–1371.

[17] M. Eichelbaum *et al.*, "The microwave cavity perturbation technique for contact-free and *in situ* electrical conductivity measurements in catalysis and materials science," *Phys. Chem. Chem. Phys.*, vol. 14, no. 3, pp. 1302–1312, Jan. 2012.

[18] M. B. Ewing and D. D. Royal, "A highly stable cylindrical microwave cavity resonator for the measurement of the relative permittivities of gases," *J. Chem. Thermodyn.*, vol. 34, no. 7, pp. 1073–1088, Jul. 2002.

[19] V. Pohl, D. Fricke, and A. Mühlbauer, "Correction procedures for the measurement of permittivities with the cavity perturbation method," *J. Microw. Power Electromagn. Energy*, vol. 30, no. 1, pp. 10–26, Nov. 1994.

[20] T. Nishikawa, K. Wakino, H. Tamura, H. Tanaka, and Y. Ishikawa, "Precise measurement method for temperature coefficient of microwave dielectric resonator material," in *IEEE MTT-S Int. Microw. Symp. Dig.*, vol. 1. May 1987, pp. 277–280.

[21] M. Mohammad-Taheri, "A simple numerical method for the calculation of temperature coefficient of resonant frequency of dielectric ring loaded cavity," in *IEEE MTT-S Int. Microw. Symp. Dig.*, Sep. 2003, pp. 431–434.

[22] H. Kawabata and Y. Kobayashi, "Accurate measurements of complex permittivity of liquid based on a TM_{010} mode cylindrical cavity method," in *Proc. 35th Eur. Microw. Conf.*, vol. 1, Oct. 2005, p. 4.

[23] P. Kanpan, E. Khansalee, N. Puangngernmak, and S. Chalermwisutkul, "TM_{010} mode cylindrical cavity for complex permittivity measurement of liquid using field analysis technique," in *Proc. 9th Int. Conf. Elect. Eng./Electron., Comput., Telecommun. Inf. Technol. (ECTI-CON)*, May 2012, pp. 1–4.

[24] M. Dietrich, D. Rauch, A. Porch, and R. Moos, "A laboratory test setup for *in situ* measurements of the dielectric properties of catalyst powder samples under reaction conditions by microwave cavity perturbation: Set up and initial tests," *Sensors*, vol. 14, no. 9, pp. 16856–16868, Jan. 2014.

[25] J. Mollá, A. Ibarra, J. Margineda, J. M. Zamarro, and A. Hernández, "Dielectric property measurement system at cryogenic temperature and microwave frequencies," *IEEE Trans. Instrum. Meas.*, vol. 42, no. 4, pp. 817–821, Aug. 1993.
[26] K. Chang and L. H. Hsieh, *Microwave Ring Circuits and Related Structures*. Hoboken, NJ, USA: Wiley, 2004.
[27] D. M. Pozar, *Microwave Engineering*. Hoboken, NJ, USA: Wiley, 2004.

Jerome A. Cuenca received the B.Eng. degree in electronic and communications engineering and Ph.D. degree in microwave materials science from Cardiff University, Cardiff, U.K., in 2012 and 2016, respectively.

He is currently a Research Associate with the School of Engineering, Cardiff University. His current research interests include applying microwave measurement techniques to characterize carbon nanomaterials, iron oxide powders, photo-reactive pigments, and 3-D printed thermoplastics.

Daniel R. Slocombe received the Ph.D. degree in electronic engineering from Cardiff University, Cardiff, U.K., in 2012.

From 2002 to 2006, he was an Engineer with the Royal Air Force, where he was involved in airborne radar systems, and a Research Fellow with the Inorganic Chemistry Laboratory, University of Oxford, Oxford, U.K., from 2012 to 2015. He is currently a Lecturer with the School of Engineering, Cardiff University, where he is a member of the Centre for High Frequency Engineering. His current research interests include microwave science and materials including microwave activation of catalytic processes, synthesis of functional oxides, dielectric spectroscopy, and new methods using magnetic resonance phenomena.

Adrian Porch received the M.A. degree in physics and the Ph.D. degree in low-temperature physics from Cambridge University, Cambridge, U.K., in 1989.

He is currently a Professor with the School of Engineering, Cardiff University, Cardiff, U.K., where he is a Research Leader with the Centre for High Frequency Engineering. He has 30 years of experience in applying microwave methods to measure and understand the fundamental properties of electronic materials. More recently, his techniques have been used to develop new types of electromagnetic sensors, with an emphasis on applications across different disciplines.